energies

MDPI

Article

Applying Directly Modified RDFT Method in Active Power Filter for the Power Quality Improvement of the Weak Power Grid

Rui Hou [1,*], Jian Wu [2], Huihui Song [2], Yanbin Qu [2] and Dianguo Xu [2]

[1] School of Information and Control Engineering, Qingdao University of Technology, Qingdao 266525, China
[2] School of Electrical Engineering and Automation, Harbin Institute of Technology, Harbin 150001, China; wujianhit@hotmail.com (J.W.); songhh@hitwh.edu.cn (H.S.); quyanbin@hit.edu.cn (Y.Q.); xudiang@hit.edu.cn (D.X.)
* Correspondence: hourui@qut.edu.cn; Tel.: +86-178-6272-2835; Fax: +86-532-8687-5010

Received: 27 August 2020; Accepted: 14 September 2020; Published: 17 September 2020



Abstract: The recursive discrete Fourier transformation (RDFT) method can be used for grid voltage phase-locking and harmonic current detection in a shunt active power filter (SAPF). However, in weak power grids such as microgrids, significant errors might occur in the amplitude and phase detection due to grid frequency deviation. In this study, to resolve this problem, a directly modified RDFT (DMRDFT) method is proposed for SAPF weak grid application. Through theoretical analysis, the errors of phase and amplitude detection were found to consist of fixed error and fluctuating error. The fixed error is only determined by frequency deviation, whereas the fluctuating error is also related to the recursive pointer and the initial phase. The DMRDFT algorithm can obtain the real grid frequency through the calculation of the phase angle difference for two consecutive periods. Then it can employ the grid frequency deviation and the recursive pointer value to directly correct the detection results gathered by the conventional RDFT algorithm. As a result, DMRDFT can yield accurate amplitude and phase information of the grid voltage or current with a simple calculation. Simulation results verify the high precision of the proposed DMRDFT method in both steady and dynamic situations. Experimental results show that the DMRDFT method can significantly increase the SAPF compensation performance when grid frequency shifts.

Keywords: power quality; power harmonic filters; microgrid; detection algorithms; error correction; discrete Fourier transforms

1. Introduction

The weak power grid, such as the microgrid, remote rural network, and poorly regulated network, is an integral part of current and future power systems [1,2]. Compared with the ordinary distribution network, the weak power grid characterized by large grid impedance suffers from more severe power quality problems such as voltage and frequency fluctuation, harmonics, imbalance [3,4]. These power quality issues may cause a series of hazards such as the abnormal operation of the sensitive load, additional losses of the electric power equipment and the reduction of their service life, the decline of the power transmission efficiency, and interference in communication [5,6]. Therefore, power quality problems in the weak power grid should be well handled. Among the several power quality improvement measures, the shunt active power filter (SAPF), based on the principle of the controlled current source, provides a flexible and effective solution for the weak grid [6–8]. It can inject a compensation current characterized by the equal amplitude and the opposite phase compared with the load-side reactive and harmonic current to ensure the grid-side unity power factor and sinusoidal current. Due to merits such as having no need for load reform, good compensation

performance, insensitivity to power grid parameters, and small resonance risk with capacitive components, the SAPF has been widely used and studied on the topology, harmonic detection method, and control strategy [9–11]. However, when the SAPF is used in the weak power grid, synchronous phasor measurement, the SAPF critical link consisting of the grid phase tracking and harmonic current detection, suffers from accuracy problems, which may significantly deteriorate SAPF compensation performance [12]. The main reason for this problem is that in the weak power grid, the frequency may fluctuate with a considerable deviation from the rated value, and the grid voltage may distort significantly [13]. These two adverse factors lead to dramatic performance reduction for the synchronous phasor measurement methods commonly used in the ordinary distribution network [12]. Accordingly, the practical method of synchronous phasor measurement becomes of interest and critical for SAPF weak grid applications.

According to current research results, the SAPF synchronous phasor measurement method can be roughly classified into two categories. One is the phase-locked loop (PLL) based method, which employs PLL to track the weak grid phase and obtain the accurate compensation current reference. Synchronous-reference frame phase-locked loop (SRF-PLL), based on a proportional-integral (PI) regulator, is the common-used PLL in the SAPF. However, much of the literature indicated that although the SRF-PLL with well-designed PI parameters could robustly operate in the frequency deviation situation, its performance would significantly suffer when grid voltage distorts, which might not be suitable for weak grid applications [14–22]. To improve the PLL performance in distorted grid voltage situations, a well-designed filter, such as the moving average filter [18,22–24], adaptive notch filter [15,25–27], was introduced in the PLL to restrain the harmonic. Unfortunately, using this approach, it is rather difficult to balance the contradiction of the system bandwidth and the harmonic rejection performance, and the PLL response speed for the frequency fluctuation suffers greatly [20]. Some other improved PLL methods have been proposed to deal with the harmonic problem, such as decoupled-network PLL [21], multiple second-order generalized integrator based PLL [28,29], hybrid PLL (HPLL) [30], the enhanced generalized delayed signal cancellation PLL (EGDSC-PLL) [31], weighted least squares estimation PLL(WLSE-PLL) [14]. Although these methods can work in distorted grid situations, the contradiction of the response speed and the harmonic rejection performance still exists and increases the difficulty of PLL design. Moreover, the implementation of these methods is quite time-consuming, which might limit their practical applications [20].

Another synchronous phasor measurement method of the SAPF is the recursive discrete Fourier transformation (RDFT) based method. Compared with the PLL-based method, the notable advantage of the RDFT-based method is that RDFT has an outstanding anti-harmonic-interference capability and can directly obtain the grid phase information without the need for the PLL in the SAPF system. Moreover, considering that the SAPF usually adopts a selective harmonic compensation strategy in practical applications to avoid resonance with the capacitive load, the multichannel RDFT method, characterized by simple implementation and high accuracy, is a quick and effective method to detect each order harmonic current, especially under the condition of three-phase unbalance [11]. However, the detection accuracy of the RDFT method is sensitive to grid frequency. When the RDFT-based method is utilized in the weak power grid, the grid frequency deviation significantly reduces the detection accuracy of the conventional RDFT method due to the spectrum leakage and the picket fence effect [32–37]. Under some extreme cases in the weak grid, the grid frequency deviation degree can reach ±1%, and the amplitude and phase detection results of RDFT may have large errors, which could reduce the accuracy of power factor control and harmonic suppression effect of the SAPF significantly. To improve the performance of the DFT-based method in the frequency fluctuating conditions, so far, some research achievements have been made, which are summarized as follows. Firstly, asynchronous sampling is the root cause of detection errors. Therefore, if the sampling rate varies with the changing of the power grid frequency, the detection result of DFT can be accurate [38]. Correspondingly, a variable sample rate DFT algorithm was presented in [39,40]. This method made a deadbeat adjustment to the time window by changing the sampling rate synchronously. However, continuously varying the

sampling rate is inconvenient for the control system in practical applications, for many discrete filtering and control parameters should vary with the sampling frequency change to ensure performance and stability. Secondly, in [33,41,42], the interpolating windowed DFT was used to eliminate the errors caused by the spectrum leakage and the picket fence effect. The interpolating algorithm can eliminate errors caused by the picket fence effect, and windowing the signals can reduce the errors produced by the leakage effect. However, the interpolating algorithm requires a large number of samples, and the interpolating equation is difficult to solve. Consequently, this method is too time-consuming to be used for real-time purposes. Similarly, there are also large computation load problems in the adaptive filter based DFT algorithms proposed in [43,44], for the real-time coefficients adjustment substantially increases the computation complexity. Last but not least, in [45,46], based on frequency tracking, the authors developed a practical compensation method to improve the phasor and power measurement accuracy of the DFT algorithm. This method takes full advantage of the DFT algorithm and simply modifies the DFT results. The calculation burden is a little more than the DFT algorithm, however notable accuracy improvement is achieved. However, this method is based on the conventional DFT algorithm, whereas a recursive algorithm is needed for real-time SAPF harmonic detection and was not provided in this paper. Furthermore, the result correction algorithm for harmonic detection was not also provided in this paper. To sum up, the improved DFT methods achieved by the studies mentioned above might be unsuitable for SAPF weak power grid applications due to their own limitations.

In this study, to achieve a fast, robust, and simply-implemented synchronous phasor measurement, a directly modified RDFT (DMRDFT) method is proposed for SAPF weak grid application. The DMRDFT method can obtain the real grid frequency without the need for PLL and directly correct the detection results gathered by the conventional RDFT algorithm with a small computation load. The proposed multichannel DMRDFT scheme can achieve dynamic phase tracking and accurate harmonic current detection simultaneously, even under grid frequency fluctuation and voltage distortion situations.

Until now, according to the knowledge of the author, there is almost no related study on the improved RDFT for SAPF weak power grid applications. The main contributions of this study lie in the following aspects.

Firstly, the generation principle and quantitative analysis of the conventional RDFT detection error for SAPF weak power grid applications are studied in detail, which might provide theoretical reference for other research on the RDFT modification strategy.

Then, a DMRDFT method is proposed to improve the SAPF real-time detection accuracy in the weak power grid. The proposed method, with a small calculation load, employs the fixed sampling rate and corrects the conventional RDFT results directly to reduce the detection errors caused by grid frequency fluctuation significantly. The main advantage of the proposed method is that it is straightforward, fast, and robust.

Last but not least, a multichannel DMRDFT scheme is proposed to track the grid phase and detect the accurate harmonic current simultaneously. Due to the elimination of extra complex PLL, the proposed scheme can ease the pressure of the SAPF control system.

This paper is organized as follows. In Section 2, the generation principle of RDFT error in the weak power grid is firstly analyzed. Then, in Section 3, the DMRDFT method for the SAPF weak power grid applications is presented. After that, detailed simulation and experimental results are provided to examine the validity of the proposed method in Section 4. Finally, the result discussions are conducted in Section 5.

2. Generation Principle of RDFT Error in Weak Power Grid

2.1. Principle of RDFT

Compared with DFT, the main advantage of RDFT lies in its simple calculation, which is conducive to real-time applications. Firstly, the principle of RDFT is briefly analyzed. The signal to be detected can be expressed as:

$$x_k(t) = \sqrt{2}Y_k \cos(k\omega t + \varphi_k) \tag{1}$$

where the signal x can be grid voltage for phase-locking or load current for harmonic detection in this study; k is the order of the harmonic; ω is the fundamental angle frequency; Y_k is the root mean square (RMS) value of the signal; φ_k is the initial phase of the signal.

RDFT is derived from DFT. Define N as the sampling number in one DFT calculation cycle, which is equal to one industrial frequency period. X_k^0 is the vector corresponding to the sampling set $\{x_k(n)\}(n = 0, 1, \dots N-1)$. More generally, corresponding to the sampling set $\{x_k(n)\}(n = r, r+1, \dots r+N-1)$, the vector turns to be X_k^r, where r is the recursive pointer. The origin of the time coordinate axis corresponds to the beginning terminal of the sampling data. According to the definition of DFT, we can obtain:

$$X_k^r = \sum_{n=0}^{N-1} x_k(r+n)e^{-j\frac{2k\pi}{N}(r+n)} \tag{2}$$

$$X_k^{r-1} = \sum_{n=0}^{N-1} x_k(r+n-1)e^{-j\frac{2k\pi}{N}(r+n-1)} \tag{3}$$

The following equation can be easily obtained:

$$X_k^r = X_k^{r-1} + [x_k(r+N-1) - x_k(r-1)]e^{-j\frac{2k\pi}{N}(r-1)} \tag{4}$$

If grid frequency is fixed at the rated frequency, obviously:

$$X_k^r = X_k^{r-1} = \cdots\cdots = X_k^0 \tag{5}$$

Unlike the conventional DFT method, in which the phase angle moves clockwise $2k\pi/N$ radian every step, in this algorithm, the phase angle of X_k^r remains invariant. Consequently, it is called recursive DFT.

2.2. RDFT Error Analysis in the Weak Power Grid

In the weak power grid, the phase angle of X_k^r rotates when grid frequency fluctuates. In this case, both the amplitude and the phase measurement results of RDFT are inaccurate. Define the auxiliary variable δ as:

$$\delta = \frac{Nf}{f_s} = \frac{N(f_0 + \Delta f)}{f_s} = 1 + \frac{\Delta f}{f_0} = 1 + \Delta\delta \tag{6}$$

where f_0 is the rated frequency of the weak grid; f is the actual frequency of the weak grid; f_s is the sampling frequency of RDFT.

The discrete signal of the data section corresponding to the vector X_k^r is:

$$x_k(r+n) = \sqrt{2}Y_k \cos(\frac{2k\pi(r+n)}{N}\delta + \varphi_k) \tag{7}$$

From Euler's formula, Equation (7) can be transformed into the complex field as:

$$x_k(r+n) = \frac{1}{\sqrt{2}}(Y_k e^{j\varphi_k} e^{j\frac{2k\pi(r+n)}{N}\delta} + Y_k e^{-j\varphi_k} e^{-j\frac{2k\pi(r+n)}{N}\delta}) \tag{8}$$

Take Equation (8) into Equation (2), and the sum symbol can be eliminated using the following formula:

$$\sum_{n=0}^{N-1} e^{-jn\alpha} = \frac{\sin(\frac{\alpha N}{2})}{\sin(\frac{\alpha}{2})} e^{-j\frac{N-1}{2}\alpha} \tag{9}$$

The result of simplification can be obtained as:

$$\begin{aligned} X_k^r &= \frac{1}{\sqrt{2}} U_k (P+Q) \\ P &= \frac{\sin(k\Delta\delta\pi)}{\sin(\frac{k\Delta\delta\pi}{N})} e^{j\varphi_k} e^{j(\frac{2\pi kr\Delta\delta}{N} + \frac{N-1}{N}k\Delta\delta\pi)} \\ Q &= \frac{\sin(k\Delta\delta\pi)}{\sin(\frac{(2+\Delta\delta)k\pi}{N})} e^{-j\varphi_k} e^{-j(\frac{4\pi kr}{N} + \frac{N-1}{N}k(2+\Delta\delta)\pi + \frac{2\pi kr}{N}\Delta\delta)} \end{aligned} \tag{10}$$

If the grid frequency is rated ($\Delta\delta = 0$), the result of RDFT is:

$$X_k^r = \frac{1}{\sqrt{2}} Y_k \lim_{\Delta\delta\to 0} \left(\frac{\sin(k\Delta\delta\pi)}{\sin(\frac{k\Delta\delta\pi}{N})} e^{j\varphi_k} e^{j(\frac{2k\pi r\Delta\delta}{N} + \frac{N-1}{N}k\Delta\delta\pi)}\right) = \frac{N}{\sqrt{2}} Y_k e^{j\varphi_k} \tag{11}$$

From Equation (11), it is denoted that the RDFT result is accurate when grid frequency is rated. In order to analyze errors when grid frequency fluctuates, an auxiliary vector is introduced:

$$F_k e^{j\beta_k} = 1 + \frac{\sin(\Delta\delta k\pi/N)}{\sin(\frac{(2+\Delta\delta)k\pi}{N})} e^{j(-2\varphi_k - \frac{4k\pi r}{N} - \frac{4k\pi r}{N}\Delta\delta - \frac{N-1}{N}2\pi k(\Delta\delta+1))} \tag{12}$$

Extracting the common factor for Equation (10), the result is:

$$X_k{}^r = \frac{1}{\sqrt{2}} Y_k \frac{\sin(k\Delta\delta\pi)}{\sin(\frac{k\Delta\delta\pi}{N})} e^{j\varphi_k} e^{j(\frac{2k\pi r\Delta\delta}{N} + \frac{N-1}{N}k\Delta\delta\pi)} F_k e^{j\beta_k} \tag{13}$$

The auxiliary vector introduced in Equation (12) is the sum of a unit vector and another vector, which is shown in Figure 1.

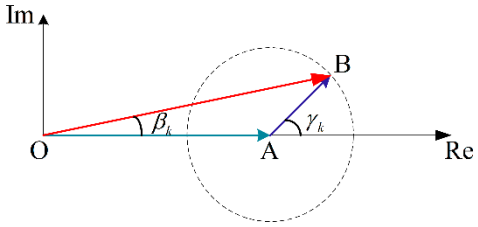


Figure 1. Auxiliary vector.

The vector $\vec{OA}$ is a unit vector, $\vec{OB}$ is an auxiliary vector $F_k e^{j\beta_k}$. The track of point B is a circle with the center at point A. The amplitude and phase angle of the vector $\left|\vec{AB}\right|$ is:

$$X_k{}^r = \frac{1}{\sqrt{2}} Y_k \frac{\sin(k\Delta\delta\pi)}{\sin(\frac{k\Delta\delta\pi}{N})} e^{j\varphi_k} e^{j(\frac{2k\pi r\Delta\delta}{N} + \frac{N-1}{N}k\Delta\delta\pi)} F_k e^{j\beta_k} \tag{14}$$

$$\gamma_k = -2\varphi_k - \frac{4k\pi r}{N} - \frac{4k\pi r}{N}\Delta\delta - \frac{N-1}{N}2\pi k(\Delta\delta+1) \tag{15}$$

The relation between β_k and γ_k is:

$$\tan\beta_k = \frac{\left|\vec{AB}\right|\sin\gamma_k}{1+\left|\vec{AB}\right|\cos\gamma_k} \tag{16}$$

Because $\left|\vec{AB}\right| = 1$ and β_k is very small, an approximation for calculating β_k is:

$$\beta_k \approx \tan\beta_k \approx \left|\vec{AB}\right|\sin\gamma_k \tag{17}$$

The approximation for calculating the amplitude of $\vec{OB}$ is:

$$F_k = \left|\vec{OB}\right| \approx 1 + \left|\vec{AB}\right|\cos\gamma_k \tag{18}$$

Define $\varphi_{km}(r)$ as the measurement result of the initial phase, the relationship between $\varphi_{km}(r)$ and φ_k is:

$$\begin{array}{l} \Delta\varphi_k = \varphi_{km} - \varphi_k = H + D \\ H = \frac{N-1}{N}\Delta\delta k\pi \\ D = \frac{2k\pi r\Delta\delta}{N} + \beta_k \end{array} \tag{19}$$

It can be seen in (19) that errors exist for phase measurement. There are two kinds of errors: one is fixed error H, which only relates to $\Delta\delta$ and k; the other one is fluctuating error D, which is influenced by r and φ_k. Another conclusion can be acquired that the error of the RDFT phase detection increases with the increase in harmonic order. For example, when $\Delta\delta$ = 0.01 and $N = 320$, the phase error is 1.79° for the fundamental wave, which may slightly affect the power control, and 23.3° for 13th harmonic, which may worsen the SAPF compensation effect seriously.

Define Y_{km} as the amplitude measurement result. Similarly, the amplitude measurement error can be obtained:

$$\Delta Y_k = \frac{Y_{km}}{NY_k/\sqrt{2}} = \frac{F_k\sin(\Delta\delta k\pi)/\sin(\Delta\delta k\pi/N)}{N} \tag{20}$$

3. Proposed DMRDFT Method

3.1. The Control Scheme of the SAPF

The control scheme of a 3p3w SAPF adopted in this study is shown in Figure 2. The SAPF control system comprises several functional modules such as the phase-locking module, harmonic current detection module, reactive power current detection module, DC voltage control module, SAPF current control module.

In this study, the SAPF selective compensation strategy is adopted due to its flexibility and low risk of resonance with the capacitive load. Accordingly, a multichannel DMRDFT scheme is proposed in the SAPF to achieve both phase-locking and harmonic current detection functions. One RDFT channel using the positive-sequence voltage u_a^+ as input obtains the grid phase and the real frequency information. The phase information is provided for the SAPF reactive power control and DC voltage control modules, and the frequency information is offered for the harmonic current detection module, which consists of several other DMRDFT channels. These channels extract the main order harmonic currents from the load current, such as the 5th, 7th, 11th, and 13th harmonics. These RDFT channels employ the real frequency information to modify the detection error caused by the frequency fluctuation directly. The harmonic current, reactive power current, and the DC voltage control current constitute the complete SAPF current reference, which is provided for the current feedback control. Modules other than DMRDFT are not the focus of this study.

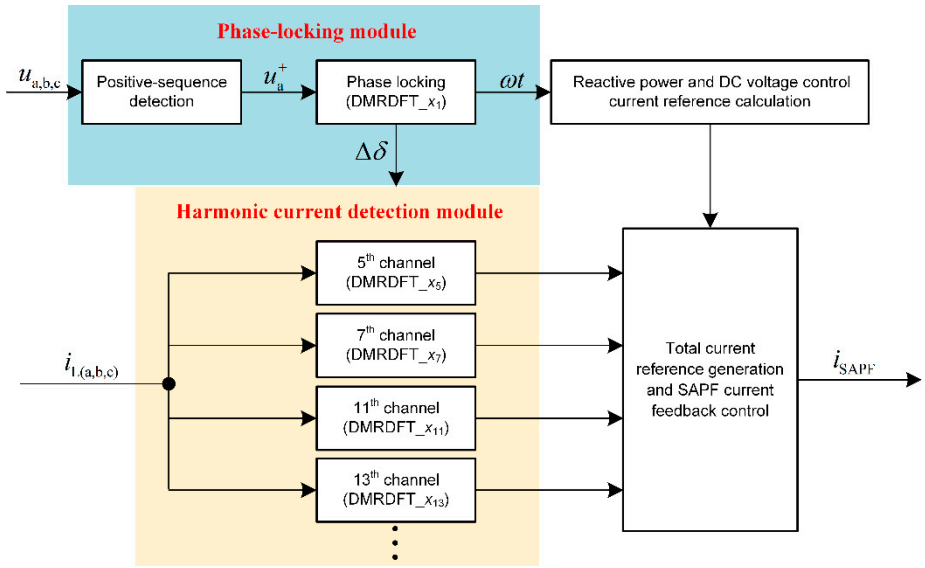


Figure 2. The proposed shunt active power filter (SAPF) control scheme.

The accumulation of round-off error is the chief deficiency of the RDFT method. In order to resolve this problem, in this study, DFT results are inserted into the RDFT calculation at the time $t = z/f_0$ ($z = 0, 1, 2 \ldots$). At these time points, r equals 1 and circulates from 1 to N in every DFT period, which is depicted in Figure 3. By this method, the round-off error of RDFT can be cleared to zero at the beginning of every DFT period, which prevents errors from accumulating.

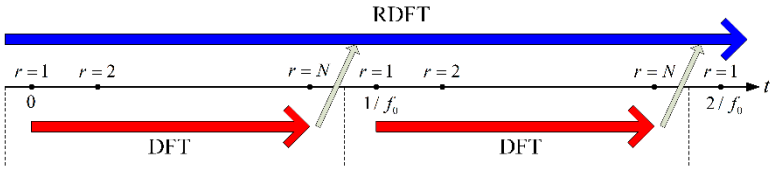


Figure 3. The method to prevent round-off error accumulation.

3.2. DMRDFT Method for Grid Frequency Tracking

In order to modify the detection error of RDFT, the grid actual fundamental frequency should be tracked accurately, which is achieved by one phase-locking functional RDFT channel corresponding to the channel DMRDFT_x_1 in Figure 2. Using the phase-detection messages of RDFT, the actual grid frequency can be measured in real time. The fluctuation of the grid frequency is caused by the imbalance between the input and output power of generators. Because the rotary inertia of the generator is quite large, the grid frequency changes continuously and slowly, and it can be assumed that the grid frequency remains unchanged in two consecutive RDFT periods. Considering that the influence of the grid harmonic on RDFT measurement results is periodic, two pieces of measured phase data from the vectors one DFT period apart can be employed to calculate the grid frequency, restraining the adverse effect of the grid harmonic significantly.

On the one hand, if no DFT result is inserted into RDFT, X_1^r and X_1^{r-N} correspond to the same initial phase angle. Define the range of phase difference as $[-\pi, \pi)$. According to (19), it can be obtained from the following equation:

$$\varphi_1 = \varphi_{1m}(r) - \frac{2\pi r\Delta\delta}{N} - \frac{N-1}{N}\Delta\delta\pi - \beta_1(r) \tag{21}$$

$$\varphi_1 = \varphi_{1m}(r-N) - \frac{2\pi (r-N)\Delta\delta}{N} - \frac{N-1}{N}\Delta\delta\pi - \beta_1(r-N) \tag{22}$$

There is a problem in that β_1 is the function of $\varphi_{1,}$ and φ_1 is unknown. An approximation can be obtained by neglecting β_k in Equation (19) as:

$$\varphi_{km}(r) \approx \varphi_k + \frac{2k\pi r\Delta\delta}{N} + \frac{N-1}{N}\Delta\delta k\pi \tag{23}$$

Based on Equation (23), the following approximations are acquired:

$$\beta_k(r) \approx \frac{\sin(\Delta\delta k\pi/N)}{\sin((2+\Delta\delta)k\pi/N)}\sin(-2\varphi_{km} - \frac{4k\pi r}{N} + \frac{2k\pi}{N}) \tag{24}$$

$$F_k(r) \approx 1 + \frac{\sin(\Delta\delta k\pi/N)}{\sin((2+\Delta\delta)k\pi/N)}\cos(-2\varphi_{km} - \frac{4\pi kr}{N} + \frac{2k\pi}{N}) \tag{25}$$

Because $\Delta\delta$ is very small, Equation (24) can be further simplified when k equals 1 as:

$$\beta_1(r) \approx \frac{\Delta\delta}{2}\sin(-2\varphi_{1m}(r) - \frac{4\pi r}{N} + \frac{1}{N}2\pi) \tag{26}$$

By Equations (21), (22) and (26), φ_1 can be eliminated, and the grid frequency calculation formula is:

$$\Delta\delta = \frac{2(\varphi_{1m}(r) - \varphi_{1m}(r-N))}{4\pi + \sin(\frac{2\pi}{N} - \frac{4\pi r}{N} - 2\varphi_{1m}(r)) - \sin(\frac{2\pi}{N} - \frac{4\pi r}{N} - 2\varphi_{1m}(r-N))} \tag{27}$$

$$f = f_0(1+\Delta\delta) \tag{28}$$

On the other hand, if the DFT results are inserted into RDFT as shown in Figure 3, X_1^r and X_1^{r-N} correspond to the different initial phase angles which are $2\pi\Delta\delta$ apart. Meanwhile, the part of $2\pi(r-N)\Delta\delta/N$ in Equation (22) should be replaced by $2\pi r\Delta\delta/N$. After derivation, it is evident that the conclusions are the same as the situation without DFT insertion.

3.3. Direct Modification Strategy of RDFT

As is depicted in Figure 2, one RDFT channel corresponding to the vector X_k (k = 1) is used to achieve the PLL function, and the other several RDFT channels corresponding to the vector X_k (k = 5, 7, 11, 13) are employed to achieve selective harmonic current detection. When the real grid frequency is acquired, the initial phase detection error of these RDFT channels can be directly modified by:

$$\Delta\varphi_k = \varphi_{km} - \varphi_k = \frac{2k\pi r\Delta\delta}{N} + \frac{N-1}{N}\Delta\delta k\pi + \beta_k(r) \tag{29}$$

The accurate amplitude of the signal is:

$$\sqrt{2}Y_k = \frac{2}{N}\frac{Y_{km}}{\Delta Y_k} \tag{30}$$

The DMRDFT method can be formulated by Equations (29) and (30). Furthermore, another DMRDFT method formulation is provided here. For kth harmonic detection, a sine reference signal $\sin[2k\pi(r-1)/N]$ and a cosine reference signal $\cos[2k\pi(r-1)/N]$, which correspond to the frequency of the detected harmonic, should be generated by the controller. Define:

$$A = \frac{2}{N}\sum_{n=0}^{N-1} x(n)\cos\frac{2k\pi n}{N} \tag{31}$$

$$B = \frac{2}{N}\sum_{n=0}^{N-1} x(n)\sin\frac{2k\pi n}{N} \tag{32}$$

The implementation process of RDFT in the time domain is:

$$A_k(r) = A_k(r-1) + \frac{2}{N}[x_k(r) - x_k(r-N)]\cos\frac{2k\pi}{N}(r-1) \tag{33}$$

$$B_k(r) = B_k(r-1) + \frac{2}{N}[x_k(r) - x_k(r-N)]\sin\frac{2k\pi}{N}(r-1) \tag{34}$$

The measured phase and magnitude information by the RDFT are:

$$\tan\varphi_{\mathrm{m}} = \frac{\mathrm{Im}[\boldsymbol{X}^r]}{\mathrm{Re}[\boldsymbol{X}^r]} = -\frac{B(r)}{A(r)} \tag{35}$$

$$\left|\boldsymbol{X}^r\right| = \sqrt{A(r)^2 + B(r)^2} \tag{36}$$

The value of φ_{m} depends on the quadrant of point [A(r), −B(r)]. If no correction is adopted, the harmonic detection result of the RDFT is:

$$y(r)_{km} = A_k(r)\cos\frac{2k\pi}{N}(r-1) + B_k(r)\sin\frac{2k\pi}{N}(r-1) \tag{37}$$

By introducing the auxiliary angle formula, Equation (37) can be transformed into:

$$y(r)_{km} = \cos(k\omega_0 t + \varphi_{km})\big|_{t=\frac{1}{f_0}+(r-1)T_s} \tag{38}$$

Whereas the actual signal is:

$$y(r)_k = \cos(k(\omega_0 + \Delta\omega)t + \varphi_k)\big|_{t=\frac{1}{f_0}+(r-1)T_s} \tag{39}$$

By moving the reference signal left, the measurement result can be corrected accurately. The correction angle for the reference signal can be obtained by contrasting Equations (38) and (39):

$$\Delta\phi_k(r) = \frac{N-1}{N}k\pi\Delta\delta - \beta_k(r) \tag{40}$$

Finally, the DMRDFT formula for the selective harmonic detection is:

$$y_k(r) = \frac{Y_{km}}{\Delta Y_k}[A_k(r)\cos(\frac{2k\pi}{N}(r-1) + \Delta\phi_k(r)) + B_k(r)\sin(\frac{2k\pi}{N}(r-1) + \Delta\phi_k(r))] \tag{41}$$

The phase-locking output result of the weak grid can be obtained by the information of φ_{m}, or can be a unit fundamental signal with the synchronous phase of u_a^+, which is provided in Equation (42).

$$y_1(r) = \frac{A_1(r)\cos(\frac{2\pi}{N}(r-1) + \Delta\phi_1(r)) + B_1(r)\sin(\frac{2\pi}{N}(r-1) + \Delta\phi_1(r))}{\sqrt{A_1(r)^2 + B_1(r)^2}} \tag{42}$$

4. Simulations and Experiments

4.1. Simulations for the DMRDFT Method

In order to verify the validity of the proposed DMRDFT method, simulations based on Matlab Simulink software were conducted.

Firstly, the steady performance of grid frequency tracking is provided. The relative simulation parameters are: the RMS value of grid line voltage is 380 V; fundamental grid frequency is 49.5 Hz; rated frequency is 50 Hz; sampling frequency of the RDFT is 16 kHz; N is 320 accordingly.

Figure 4a provides the steady grid frequency tracking performance of the DMRDFT method when no harmonic exists. The precision of frequency tracking is within 0.0001 Hz. Figure 4b shows the tracking effect when the 5th harmonic exists with an amplitude of 20 V. Although the measurement precision decreases, the error is still within 0.005 Hz, which can meet the actual needs. Moreover, it can be noticed that the fluctuation frequency of measurement error is two times that of the grid frequency, and the measurement error might be attributed to the approximation in the derivation process.

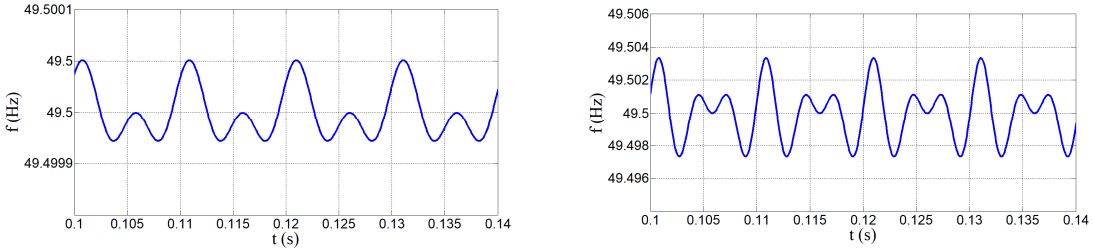


Figure 4. Steady effect on frequency tracking of the directly modified recursive discrete Fourier transformation (DMRDFT): (**a**) performance when without harmonic, and (**b**) performance when with harmonic.

Based on the same simulation parameters, the phase correction effect of DMRDFT on fundamental voltage detection is shown in Figure 5. It is noted that the conventional RDFT method induces a fixed error with a value of 1.8 degrees and a fluctuation error with a frequency of 100 Hz. After being directly modified, the phase error is substantially reduced. When no harmonic exists, the precision is within 0.01 degrees; when the fifth harmonic is included, the precision still reaches 0.1 degrees, which can meet the actual demands.

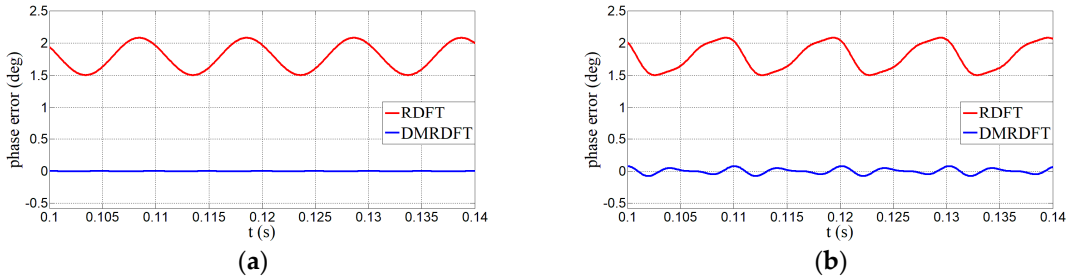


Figure 5. Steady performance comparison of grid voltage phase tracking: (**a**) performance when without harmonic, and (**b**) performance when with harmonic.

The amplitude correction effect of DMRDFT is shown in Figure 6. Compared with the conventional RDFT method, the amplitude error is significantly reduced by using the DMRDFT method. When no harmonic exists, the error is within 0.01 V; when the fifth harmonic is included, the error is within ±0.5 V, which is acceptable in practical applications.

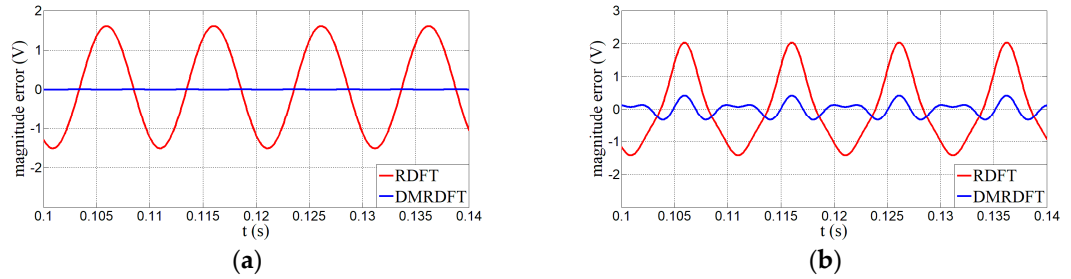


Figure 6. Steady performance comparison of grid voltage magnitude tracking: (**a**) performance when without harmonic, and (**b**) performance when with harmonic.

Secondly, the dynamic effect on grid frequency tracking was verified. In order to simulate the continuous and slow change of grid frequency, the grid voltage is supposed to change according to the laws of the slope. Because the angular frequency is the derivative of the phase, we can make grid frequency vary in a particular law by changing the initial phase of grid voltage. In the simulation, the grid frequency decreases at the rate of 0.3 Hz/s after 0.1 s and increases at the rate of 0.25 Hz/s after 1.1 s. Moreover, the fifth harmonic is included, whose amplitude is 5% of that of the fundamental wave. As is shown in Figure 7, the dynamic effect on frequency tracking is satisfactory, even if the harmonic exists. Because the frequency is understood to remain constant in two consecutive periods, measurement frequency has a delay of 0.04 s compared with actual frequency. However, actual grid frequency changes quite slowly, so the dynamic precision of DMRDFT can meet the actual needs well. Figure 8 shows the dynamic effect on phase tracking of grid voltage when the fifth harmonic exists. As is shown, phase errors of the conventional RDFT method are large with a fluctuation component, whereas the errors of DMRDFT are within 0.1 degrees even if the harmonic exists.

In order to verify the detection precision of the DMRDFT method for harmonic current, corresponding simulations were performed. The relative parameters are: the real grid fundamental frequency is 49.5 Hz; the sampling frequency is 16 kHz; N equals 320 accordingly. Figures 9 and 10 show the phase and amplitude correction effect on detecting the 5th and 17th harmonic currents with an amplitude value of 1 A.

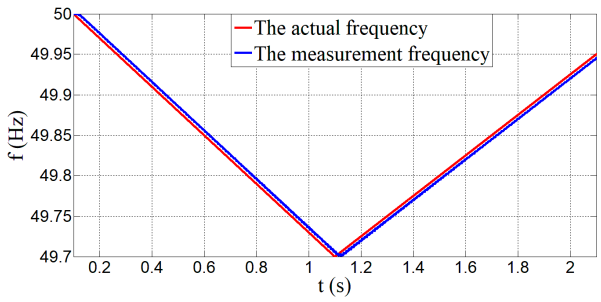


Figure 7. Dynamic effect on frequency tracking of DMRDFT with the harmonic.

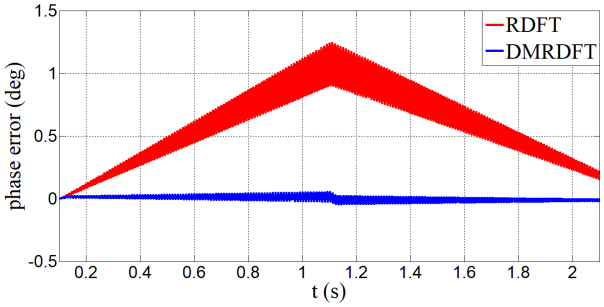
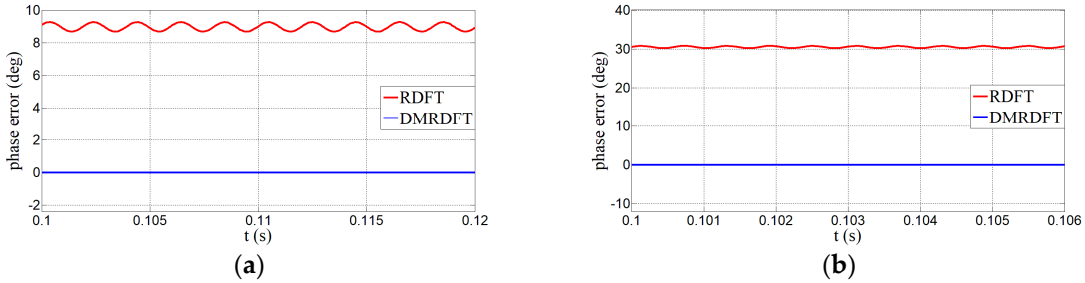


Figure 8. Dynamic effect on phase tracking with the harmonic.



(**a**) (**b**)

Figure 9. Correction effect on selective harmonic phase detection: (**a**) 5th harmonic (k = 5), and (**b**) 17th harmonic (k = 17).

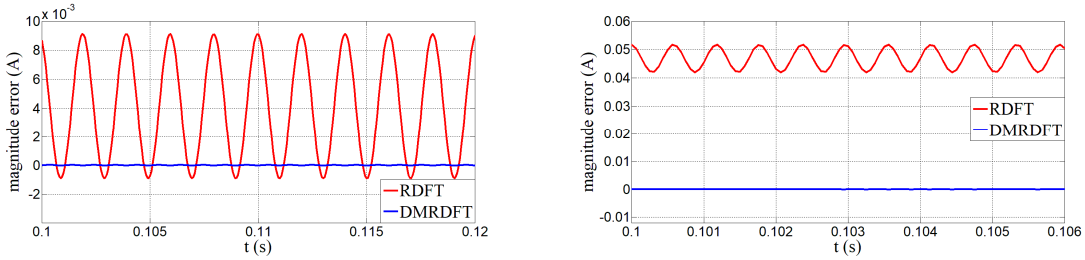


Figure 10. Correction effect on selective harmonic magnitude detection: (**a**) 5th harmonic (k = 5), and (**b**) 17th harmonic (k = 17).

From Figures 9 and 10, it is noted that grid frequency fluctuation harms detecting harmonic current when the conventional RDFT method is used, especially for phase detection. The detection error enlarges with the harmonic order increase. For the 17th harmonic, the constant phase error can reach about 30 degrees when the grid frequency deviation is 0.5 Hz, and the amplitude detection error also reaches 4%. Whereas, using the DMRDFT method, the phase and amplitude detection errors are both approximately zero, which verifies the validity of the proposed method.

In order to verify the dynamic correction effect on harmonic current detection, the slope response test was performed. In the simulation, the grid frequency decreases at the rate of 0.3 Hz/s after 0.1 s and increases at the rate of 0.25 Hz/s after 1.1 s. Meanwhile, the multifarious harmonic is mixed to simulate actual situations. The mixed harmonic current comprises the orders of 5th, 7th, 11th, 13th, 17th, and 19th. The constitution of the mixed harmonic current is shown in Table 1.

Here only dynamic phase error for the 17th harmonic detection is examined because it is the worst situation. As is shown in Figure 11, the DMRDFT method has a minor dynamic error compared with the RDFT method, although errors are not eliminated entirely. There are two reasons for the dynamic error of the DMRDFT method: one is that the mixture of the multifarious harmonic reduces the precision of the correction method; the other one is the delay of two RDFT periods for grid frequency tracking. Fortunately, the maximum dynamic error of the DMRDFT method is still under 25% of that of the RDFT method, which is substantially satisfactory.

Finally, to check the influence of grid voltage phase detection accuracy on the SAPF reactive-power control performance under the weak grid situation, a related simulation was conducted. In the simulation, the grid frequency is 50.5 Hz, which emulates the frequency deviation situations in the weak power grid. The grid phase is calculated by the DMRDFT method and provided for an additional instantaneous reactive power detection module. The SAPF compensates for the reactive power current and the harmonic current using the current timing-comparison control. The other related simulation parameters are: the three-phase reactive power capacity of the load is 200 kVA; the three-phase active power load is a resistor of 100 Ω; the connection reactance of the SAPF is 0.5 mH; the DC-link voltage is 760 V. Figure 12 shows the contrast of the reactive power control performance by the conventional RDFT and DMRDFT methods.

As is shown in Figure 12, the grid-side residual inductive reactive power is about 1 kVAr on average when the SAPF adopts the conventional RDFT method, and the power factor is relatively low, its lowest value is only 0.88. It is mainly because the conventional RDFT method will lead to the phase detection error of the weak grid, which reduces the reactive power control performance significantly. Furthermore, the reason why the grid-side reactive power factor is under-compensated in this situation lies in that the grid frequency is higher than the rated frequency, which induces that the detected grid phase lags behind the real phase. For the same reason, the grid-side reactive power factor is overcompensated when the grid frequency is lower than the rated frequency. In contrast, as is depicted in Figure 12, the grid-side residual reactive power is approximately zero on average when the SAPF employs the DMRDFT method, and the power factor is significantly improved; itsvalue is more likely to be to one. The improvement of the SAPF reactive power control performance benefits from

the accurate grid phase information provided by the DMRDFT method, which proves the effectiveness of the proposed DMRDFT method for the weak grid phase locking.

Table 1. Constitution of the harmonic current.

Harmonic Order	5th	7th	11th	13th	17th	19th
Amplitude(A)	30	21	14	11	9	8

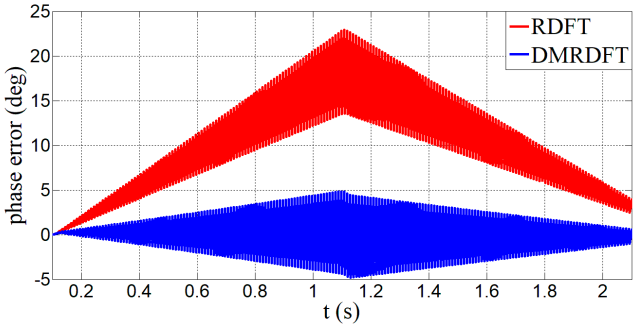


Figure 11. Dynamic phase effect on the 17th harmonic detection.

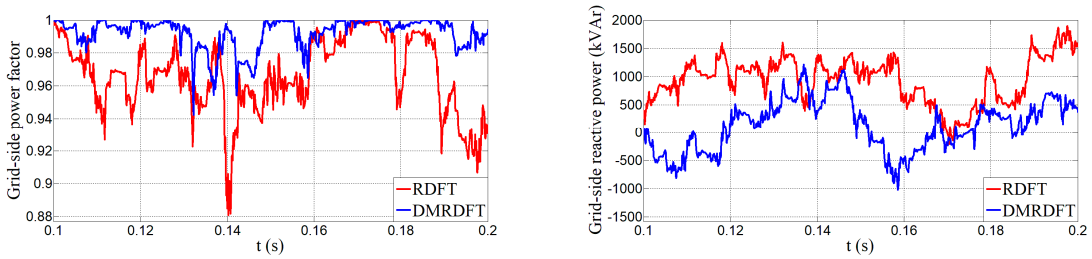


Figure 12. Contrast of the SAPF reactive power control performance: (**a**) grid-side power factor, and (**b**) grid-side residual reactive power.

4.2. Experiments for the DMRDFT Method

In order to verify the actual effect on the DMRDFT method used in the SAPF, a related experiment was conducted. A programmable power supply is used to generate grid frequency deviation and simulate the weak grid conditions. In the experiment, the grid frequency is set to 49.5 Hz, whereas the rated frequency is 50 Hz. Due to the power limit of the power supply, the low-power experiment is performed to verify the proposed algorithm, and the root mean square (RMS) value of grid line voltage is set to 50 V for the power limitation. An available SAPF prototype in the lab, which is shown in Figure 13, is used to detect and compensate the 5th, 7th, 11th, 13th harmonic current generated by a thyristor rectifier load in the grid. The connection inductance is 4 mH, and DC-link voltage is controlled to be 100 V for the SAPF. The sampling frequency of the controller is 8 kHz, and N equals 160 accordingly.

In Figure 14, the SAPF compensation effect using the RDFT and DMRDFT methods are compared. As is shown, the SAPF using the DMRDFT method obviously compensates the harmonic better; as a result, the grid current using the DMRDFT method is closer to the sine wave. The detailed measurement data of the harmonic RMS values are provided in Table 2. It is noted that the compensation effect is significantly increased by using the DMRDFT method in the situation of grid frequency deviation. The compensation effect using the conventional RDFT method is poor, especially for high order harmonics. The total harmonic distortion (THD) value of the load current is 25.2%. After compensation, the THD value of the grid current is 17.2% using the RDFT method, whereas the THD value of the grid current reaches 6.9% using the DMRDFT method, which is quite satisfactory.

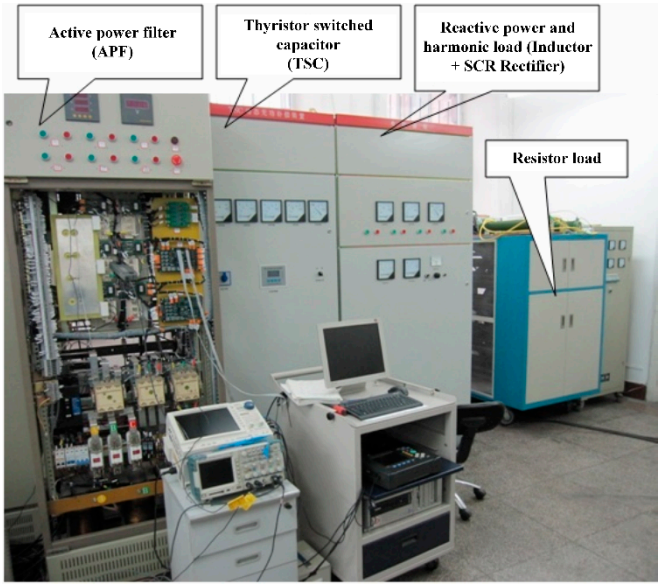


Figure 13. The SAPF prototype in the lab.

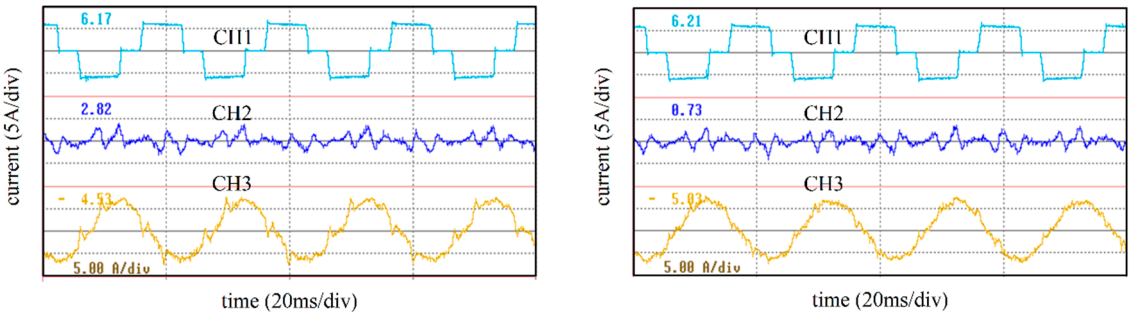


Figure 14. The SAPF compensation performance with frequency deviation: (**a**) effect using the RDFT method, and (**b**) effect using the DMRDFT method. (CH1—Load current of A phase; CH2—SAPF current of B phase; CH3—Grid current of C phase)

Table 2. The measurement result of harmonic current.

Harmonic Order	5th	7th	11th	13th
Load current RMS(A)	0.91	0.59	0.44	0.26
Grid current RMS using RDFT(A)	0.46	0.45	0.39	0.24
Grid current RMS using DMRDFT(A)	0.13	0.18	0.08	0.08

5. Discussion

Based on the simulation and experimental results, the following discussions are conducted.

5.1. Amount of Computation

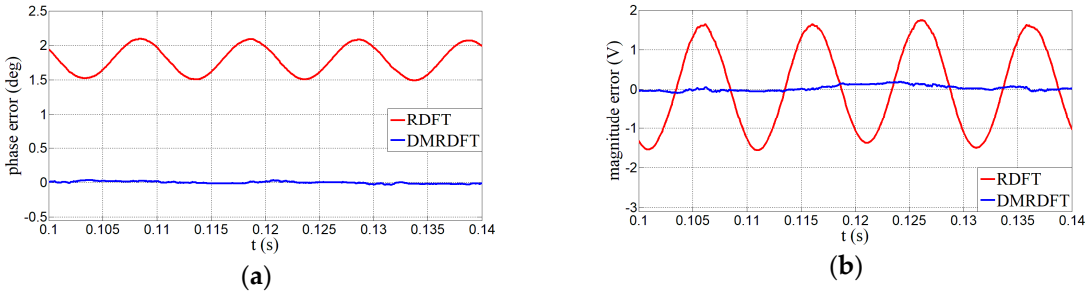
The small amount of computation is the significant advantage of the RDFT method. To overcome the error caused by frequency deviation, the DMRDFT method proposed in this paper introduces an additional two parts computation compared with the conventional RDFT method. One is the frequency estimation part, which introduces an additional six additions, seven multiplications, and two sine operations. All of the DMRDFT harmonic channels can share the frequency estimation result. The other additional computation is the phase and magnitude modification part. For each DMRDFT harmonic channel, this part introduces an extra twelve additions, eighteen multiplications, and ten sine operations. As can be seen, the computation amount of the proposed DMRDFT method is low.

Moreover, the experiment in Section 4.2 employs the digital signal processor to achieve five-channel DMRDFT detection and SAPF control, communication, and other functions easily, which also proves that the proposed DMRDFT method is easy to implement in practice.

5.2. Influence of Noise

The noise, which is inevitable in the practical environment, will deteriorate the performance of digital signal processing. In order to examine the DMRDFT performance with the environmental noise, the following simulation is conducted. A white Gaussian noise signal, whose variance is two and peak-to-peak value is 9.5 V, is added to the A phase grid voltage u_a. The phase and magnitude of u_a are calculated by the DMRDFT method, and the results are shown in Figure 15.

As is depicted in Figure 15, the noise has adverse effects on the DMRDFT detection accuracy due to the spectrum interference. Compared with the ideal case without noise, both the phase and magnitude errors increase. Nonetheless, the phase error peak value is within 0.05 degree, and the magnitude error peak value is within 0.2 V, which is still satisfactory in practice. Moreover, the experiments in Section 4.2 also prove the feasibility of the proposed DMRDFT method.

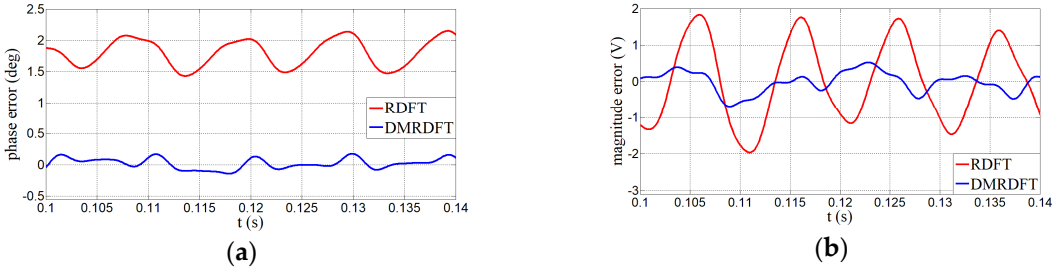


(**a**) (**b**)

Figure 15. The contrast of RDFT and DMRDFT performance with the noise: (**a**) phase error, and (**b**) magnitude error.

5.3. Influence of Interharmonics

Interharmonics, also known as noninteger harmonics, is caused by the nonlinear elements in the weak power grid such as the arc furnace and ferromagnetic materials. In order to examine the DMRDFT performance with the interharmonics background, the related simulations were performed. The interharmonic voltage superimposed on u_a comprises a 10 Hz subharmonic voltage with the amplitude of 1 V, a 160 Hz harmonic voltage with an amplitude of 3 V, and a 260 Hz harmonic voltage with an amplitude of 3 V. The phase and magnitude of u_a are detected by the DMRDFT method, and the results are illustrated in Figure 16.



(**a**) (**b**)

Figure 16. The contrast of the RDFT and DMRDFT performance with the interharmonics: (**a**) phase error, and (**b**) magnitude error.

It can be seen in Figure 16 that the interharmonics deteriorate the DMRDFT accuracy for both phase and magnitude detection. It is mainly because the interharmonics produce spectrum interference to the desired components. Nevertheless, the phase error peak value is within 0.2 degrees, and the

magnitude error peak value is within 0.7 V. Considering that the interharmonic amount is low in the real power grid, the detection accuracy of the proposed DMRDFT method is acceptable in practice.

5.4. Sensitivity Analysis

In order to evaluate the sensitivity of the DMRDFT detection accuracy to various adverse factors, a brief sensitivity analysis was conducted. The sensitivity analysis factor (SAF) is defined as:

$$\mathrm{SAF} = \frac{\Delta \mathrm{A}/\mathrm{A}}{\Delta \mathrm{F}/\mathrm{F}} \tag{43}$$

where $\Delta A/A$ means the variation ratio of the evaluation index and $\Delta F/F$ represents the variation ratio of the adverse factor. The RMS value of the phase and magnitude detection error of DMRDFT is selected as the evaluation index. The detection object of DMRDFT is a fundamental voltage with an amplitude of 100 V. Several adverse factors superimposed on the fundamental voltage consist of harmonics, interharmonics, noise, and frequency sloping change. The harmonic part comprises the 5th, 7th, 11th, 13th, 17th, 19th harmonic voltage with the amplitude of 1 V, respectively. The interharmonic part contains 0.2, 3.2, 5.2 order harmonics with the amplitude of 1 V, respectively. The variance of the white Gaussian noise signal is one. The frequency changing rate is the same as that of the simulation in Figure 7. By examining the variation rate of the evaluation index when each adverse factor increases 100% separately, the SAF can be calculated, as shown in Table 3.

Table 3. Sensitivity analysis results.

F (Adverse Factor)	ΔF/F (%)	$\lvert\Delta A_1/A_1\rvert$ (%, Phase Error)	$\lvert\Delta A_2/A_2\rvert$ (%, Magnitude Error)	$\lvert SAF_1\rvert$ (Phase Error)	$\lvert SAF_2\rvert$ (Magnitude Error)
Noise variance	200	0.1463	0.1390	0.0731	0.0695
frequency slope	100	0.0468	0.0426	0.0468	0.0426
0.2nd harmonic	100	0.7883	0.7539	0.7883	0.7539
3.2nd harmonic	100	0.0867	0.1218	0.0867	0.1218
5.2nd harmonic	100	0.0149	0.0448	0.0149	0.0448
5th harmonic	2000	0.0633	0.1287	0.0032	0.0064
7th harmonic	2000	0.0633	0.1231	0.0032	0.0062
11th harmonic	2000	0.0628	0.1192	0.0031	0.0060
13th harmonic	2000	0.0644	0.1183	0.0032	0.0059
17th harmonic	2000	0.0681	0.1166	0.0034	0.0058
19th harmonic	2000	0.0713	0.1162	0.0036	0.0058

Based on the sensitivity analysis results illustrated in Table 3, the most sensitive factor of DMRDFT accuracy is the interharmonics and subharmonics, especially the subharmonics. It is mainly because the spectrum of interharmonics interferes with the spectrum of measured frequency. Moreover, the closer the interharmonic frequency is to the measured frequency, the more serious the interference is, which is consistent with the analysis results in Table 3. Fortunately, the amount of interharmonics and subharmonics is usually relatively low, and the DMRDFT accuracy can be ensured in the real power grid. Nonetheless, how to further restrain the influence of interharmonic on the accuracy of DMRDFT still needs to be studied, and this could be the direction of the future work of this study. Furthermore, the influence of the frequency changing slope and the noise variance on the DMRDFT accuracy also cannot be ignored. The noise power spectral density and the frequency changing rate considered in this study are usually more severe than those in the real conditions. Therefore, these two adverse factors commonly will not affect the practical application performance of DMRDFT. Nevertheless, SAPF circuit systems, especially the main circuit, transmission lines, and printed circuit boards, should be well designed to reduce the noise level and improve DMRDFT performance. Last but not least, the integer harmonics have little influence on the DMRDFT performance, which benefits from the orthogonality of integer harmonic space.

6. Conclusions

This paper has made the following conclusions based on previous studies:

In a weak power grid, grid frequency often shifts, and large errors will occur for the amplitude and phase detection using the RDFT algorithm. After being analyzed, the measurement errors can be divided into fixed error and fluctuating error. For the specific harmonic, the fixed error is only determined by frequency deviation, whereas the fluctuating error is also related to the recursive pointer and the initial phase. The measurement error of grid fundamental voltage detection harms unit power factor control for the SAPF, and the measurement error of harmonic current will induce the deterioration of the SAPF compensation performance. With the increase of harmonic order, the measurement error increases significantly.

A DMRDFT method is proposed to resolve this problem in the paper. This algorithm acquires the real grid frequency through the calculation of the phase angle difference for two consecutive periods. Then it utilizes the grid frequency deviation and recursive pointer value to correct the detection results obtained from the conventional RDFT algorithm, which will yield the accurate amplitude and phase information of the grid voltage or current. A set of calculation formulas are provided to correct the measurement errors for the conventional RDFT method, and the total amount of calculation for this algorithm is quite small, which is suitable for SAPF applications.

Simulations have verified the high precision of the proposed DMRDFT algorithm in both steady and dynamic situations. In steady conditions, the frequency tracking precision of the DMRDFT method reaches 0.01 Hz, and the phase detection error is within 0.1 degrees. When the frequency shifts slowly, the DMRDFT method can track the real frequency well. Even for the mixed harmonic detection in dynamic situations, the amplitude and phase errors are significantly reduced compared with the conventional RDFT method. To a certain extent, interharmonics and noise can worsen the detection accuracy of DMRDFT. Considering that they are usually low in the real power grid, the practical DMRDFT detection accuracy can be guaranteed. Experimental results show the DMRDFT method can significantly increase the SAPF compensation performance when the grid frequency shifts.

Author Contributions: Conceptualization, R.H.; methodology, R.H.; software, R.H.; validation, R.H.; formal analysis, R.H., J.W. and H.S.; investigation, R.H., J.W. and H.S.; resources, D.X.; data curation, R.H.; writing—original draft preparation, R.H.; writing—review and editing, R.H.; visualization, R.H.; supervision, Y.Q. and D.X.; project administration, R.H and Y.Q. All authors have read and agreed to the published version of the manuscript.

Funding: This research was funded by the National Natural Science Foundation of China (No.61773137), the Natural Science Foundation of Shandong Province (Nos.ZR2019MF030 and ZR2018PEE018), China Postdoctoral Science Foundation (No.2018M641830).

Conflicts of Interest: The authors declare no conflict of interest.

Nomenclature

Abbreviations

DFT	Discrete Fourier transformation
RDFT	Recursive discrete Fourier transformation
DMRDFT	Directly modified Recursive discrete Fourier transformation
SAPF	Shunt active power filter
PI	Proportional-integral
PLL	Phase-locked loop
SRF-PLL	Synchronous-reference frame phase-locked loop
HPLL	Hybrid PLL
EGDSC-PLL	Enhanced generalized delayed signal cancellation PLL
WLSE-PLL	Weighted least squares estimation PLL
RMS	Root mean square
SAF	Sensitivity analysis factor

Variables, Parameters, and Constants

u_a, u_a^+	A-phase voltage/positive-sequence voltage of the weak power grid
x	Grid voltage for phase-locking or load current for harmonic detection
k	The order of harmonic
f, ω	The fundamental frequency/angle frequency
f_0, f_s	The rated frequency of the weak grid/sampling frequency of RDFT
Y_k, φ_k	The RMS value/initial phase of signal
N	The sampling number in one DFT calculation cycle
r	The recursive pointer
X_k^r	The vector corresponding with the sampling set $\{x_k(n)\}(n=r,r+1, \ldots\ r+N-1)$
δ	The auxiliary variable representing a relative change in frequency
F_k, β_k	The amplitude/phase angle of the auxiliary vector $F_k e^{j\beta_k}$
γ_k	The phase angle of the auxiliary vector $\left\vert\vec{AB}\right\vert$
Y_{km}, φ_{km}	The RDFT measurement result of amplitude/initial phase
H, D	The fixed/fluctuating error for RDFT phase measurement
$A_k(r)$, $B_k(r)$	RDFT process variables corresponding to cosine/sine reference signals
$y(r)_k$, $y(r)_{km}$	The actual signal/ RDFT detection harmonic result
$y_k(r)$	The DMRDFT result for the selective harmonic detection
ΔA/A, ΔF/F	The variation ratio of evaluation index/the adverse factor

References

1. Pei, J.; Yao, J.; Liu, R.; Zeng, D.; Sun, P.; Zhang, H.; Liu, Y. Characteristic Analysis and Risk Assessment for Voltage-frequency Coupled Transient Instability of Large-Scale Grid-Connected Renewable Energy Plants during LVRT. *IEEE Trans. Ind. Electron.* **2020**, *67*, 5515–5530. [CrossRef]
2. Wang, D.; Zhang, X.; Yang, L.; Huang, Y.; Huang, W.; Wu, C.; Li, S. Analysis of Synchronization Stability for Multi VSCs Parallel-Connected to Weak Grids by Improved Net Damping Criterion. *Energies* **2020**, *13*, 3316. [CrossRef]
3. Zimann, F.J.; Stangler, E.V.; Neves, F.A.S.; Batschauer, A.L.; Mezaroba, M. Coordinated Control of Active and Reactive Power Compensation for Voltage Regulation with Enhanced Disturbance Rejection Using Repetitive Vector-Control. *Energies* **2020**, *13*, 2812. [CrossRef]
4. Zhu, K.; Sun, P.; Zhou, L.; Du, X.; Luo, Q. Frequency-Division Virtual Impedance Shaping Control Method for Grid-Connected Inverters in a Weak and Distorted Grid. *IEEE Trans. Power Electron.* **2020**, *35*, 8116–8129. [CrossRef]
5. Shukl, P.; Singh, B. Delta-Bar-Delta Neural-Network-Based Control Approach for Power Quality Improvement of Solar-PV-Interfaced Distribution System. *IEEE Trans. Ind. Inform.* **2020**, *16*, 790–801. [CrossRef]
6. Geng, H.; Zheng, Z.; Zou, T.; Chu, B.; Chandra, A. Fast Repetitive Control with Harmonic Correction Loops for Shunt Active Power Filter Applied in Weak Grid. *IEEE Trans. Ind. Appl.* **2019**, *55*, 3198–3206. [CrossRef]
7. Jarwar, A.R.; Soomro, A.M.; Memon, Z.A.; Odhano, S.A.; Uqaili, M.A.; Larik, A.S. High Dynamic Performance Power Quality Conditioner for AC Microgrids. *IET Power Electron.* **2019**, *12*, 550–556. [CrossRef]
8. Singh, S.; Kewat, S.; Singh, B.; Panigrahi, B.K.; Kushwaha, M.K. BD-VSS Individual Weighting Factor Sign Based Adaptive Filter Control for Power Quality Improvement in Weak Distribution Grid. *IET Gener. Transm. Distrib.* **2020**, *14*, 1450–1457. [CrossRef]
9. Popescu, M.; Bitoleanu, A.; Suru, C.V.; Linca, M.; Subtirelu, G.E. Adaptive Control of DC Voltage in Three-Phase Three-Wire Shunt Active Power Filters Systems. *Energies* **2020**, *13*, 3147. [CrossRef]
10. Gao, Y.; Li, X.; Zhang, W.; Hou, D.; Zheng, L. A Sliding Mode Control Strategy with Repetitive Sliding Surface for Shunt Active Power Filter with an LCLCL Filter. *Energies* **2020**, *13*, 1740. [CrossRef]
11. Kumar, R.; Bansal, H.O. Shunt Active Power Filter: Current Status of Control Techniques and Its Integration to Renewable Energy Sources. *Sust. Cities Soc.* **2018**, *42*, 574–592. [CrossRef]
12. Nie, X.; Liu, J. Current Reference Control for Shunt Active Power Filters Under Unbalanced and Distorted Supply Voltage Conditions. *IEEE Access* **2019**, *7*, 177048–177055. [CrossRef]
13. Jain, V.; Singh, B. A Multiple Improved Notch Filter-Based Control for a Single-Stage PV System Tied to a Weak Grid. *IEEE Trans. Sustain. Energy* **2019**, *10*, 238–247. [CrossRef]

14. Zheng, L.; Geng, H.; Yang, G. Fast and Robust Phase Estimation Algorithm for Heavily Distorted Grid Conditions. *IEEE Trans. Ind. Electron.* **2016**, *63*, 6845–6855. [CrossRef]
15. Hui, N.; Luo, Z.; Feng, Y.; Han, X. A Novel Grid Synchronization Method Based on Hybrid Filter Under Distorted Voltage Conditions. *IEEE Access* **2020**, *8*, 65636–65648. [CrossRef]
16. Hoon, Y.; Radzi, M.A.M.; Hassan, M.K.; Mailah, N.F. Operation of Three-Level Inverter-Based Shunt Active Power Filter Under Nonideal Grid Voltage Conditions with Dual Fundamental Component Extraction. *IEEE Trans. Power Electron.* **2018**, *33*, 7558–7570. [CrossRef]
17. Tang, M.; Bifaretti, S.; Pipolo, S.; Odhano, S.; Zanchetta, P. A Novel Repetitive Controller Assisted Phase-Locked Loop with Self-Learning Disturbance Rejection Capability for Three-Phase Grids. *IEEE J. Emerg. Sel. Top. Power Electron.* **2020**, *8*, 1870–1879. [CrossRef]
18. Hui, N.; Feng, Y.; Han, X. Design of a High Performance Phase-Locked Loop With DC Offset Rejection Capability Under Adverse Grid Condition. *IEEE Access* **2020**, *8*, 6827–6838. [CrossRef]
19. Mansor, M.A.; Hasan, K.; Othman, M.M.; Noor, S.Z.B.M.; Musirin, I. Construction and Performance Investigation of Three-Phase Solar PV and Battery Energy Storage System Integrated UPQC. *IEEE Access* **2020**, *8*, 103511–103538. [CrossRef]
20. Hogan, D.J.; Gonzalez-Espin, F.J.; Hayes, J.G.; Lightbody, G.; Foley, R. An Adaptive Digital-Control Scheme for Improved Active Power Filtering Under Distorted Grid Conditions. *IEEE Trans. Ind. Electron.* **2018**, *65*, 988–999. [CrossRef]
21. Hadjidemetriou, L.; Kyriakides, E.; Blaabjerg, F. A Robust Synchronization to Enhance the Power Quality of Renewable Energy Systems. *IEEE Trans. Ind. Electron.* **2015**, *62*, 4858–4868. [CrossRef]
22. Niazi, A.N.; Vasegh, N.; Birjandi, A.A.M. To Study Unplanned Islanding Transient Response of Microgrid by Implementing MSOG and SRF-PLL Based Hierarchical Control in the Presence of Non-linear Loads. *IET Renew. Power Gener* **2020**, *14*, 881–890. [CrossRef]
23. Ramos, C.J.; Martins, A.P.; Carvalho, A.D.S. Power system frequency estimation using a least mean squares differentiator. *Int. J. Electr. Power Energy Syst.* **2017**, *87*, 166–175. [CrossRef]
24. Golestan, S.; Guerrero, J.M.; Vidal, A.; Yepes, A.G.; Doval-Gandoy, J. PLL with MAF-based prefiltering stage: Small-signal modeling and performance enhancement. *IEEE Trans. Power Electron.* **2016**, *31*, 4013–4019. [CrossRef]
25. Shin, D.; Lee, K.J.; Lee, J.P.; Yoo, D.W.; Kim, H.J. Implementation of Fault Ride-Through Techniques of Grid-Connected Inverter for Distributed Energy Resources with Adaptive Low-Pass Notch PLL. *IEEE Trans. Power Electron.* **2015**, *30*, 2859–2871. [CrossRef]
26. Pan, H.; Li, Z.; Wei, T. A Novel Phase-Locked Loop with Improved-Dual Adaptive Notch Filter and Multi-Variable Filter. *IEEE Access* **2019**, *7*, 176578–176586. [CrossRef]
27. Shitole, A.B.; Suryawanshi, H.M.; Talapur, G.G.; Sathyan, S.; Ballal, M.S.; Borghate, V.B.; Ramteke, M.R.; Chaudhari, M.A. Grid interfaced distributed generation system with modified current control loop using adaptive synchronization technique. *IEEE Trans. Ind. Inform.* **2017**, *13*, 2634–2644. [CrossRef]
28. Golestan, S.; Mousazadeh, S.Y.; Guerrero, J.M.; Vasquez, J.C. A critical examination of frequency-fixed second-order generalized integrator-based phase-locked loops. *IEEE Trans. Power Electron.* **2017**, *32*, 6666–6672. [CrossRef]
29. Xiao, F.; Dong, L.; Li, L.; Liao, X. A frequency-fixed SOGI-based PLL for single-phase grid-connected converters. *IEEE Trans. Power Electron.* **2017**, *32*, 1713–1719. [CrossRef]
30. Jain, P.; Agarwal, V.; Muni, B.P. Hybrid Phase Locked Loop for Controlling Master-Slave Configured Centralized Inverters in Large Solar Photovoltaic Power Plants. *IEEE Trans. Ind. Appl.* **2018**, *54*, 3566–3574. [CrossRef]
31. Golestan, S.; Freijedo FDVidal AYepes, A.G.; Guerrero, J.M.; Doval-Gandoy, J. An efficient implementation of generalized delayed signal cancellation PLL. *IEEE Trans. Power Electron.* **2016**, *31*, 1085–1094. [CrossRef]
32. Zhan, L.; Liu, Y.; Liu, Y. A Clarke Transformation-Based DFT Phasor and Frequency Algorithm for Wide Frequency Range. *IEEE Trans. Smart Grid* **2018**, *9*, 67–77. [CrossRef]
33. Wen, H.; Li, C.; Yao, W. Power System Frequency Estimation of Sine-Wave Corrupted With Noise by Windowed Three-Point Interpolated DFT. *IEEE Trans. Smart Grid* **2018**, *9*, 5163–5172. [CrossRef]
34. Fu, L.; Xiong, S.; Pan, C.; Bai, S.; He, Z.; Mai, R.; Li, X. A Multiple Frequency Taylor Model-based Dynamic Synchrophasor Estimation Algorithm. *IEEE Trans. Smart Grid* **2019**, *10*, 6870–6882. [CrossRef]

35. Xia, T.; Zhang, X.; Tan, G.; Liu, Y. Synchronous Reference Frame Single-phase Phase-locked Loop (PLL) Algorithm Based on Half-cycle DFT. *IET Power Electron.* **2020**, *13*, 1893–1900. [CrossRef]
36. Liu, H.; Hu, H.; Chen, H.; Zhang, L.; Xing, Y. Fast and Flexible Selective Harmonic Extraction Methods Based on the Generalized Discrete Fourier Transform. *IEEE Trans. Power Electron.* **2018**, *33*, 3484–3496. [CrossRef]
37. Xie, X.; Zhan, Y.; Liu, H.; Liu, C. Improved Synchrophasor Measurement to Capture Sub/super-Synchronous Dynamics in Power Systems with Renewable Generation. *IET Renew. Power Gener.* **2019**, *13*, 49–56. [CrossRef]
38. Yamada, T. High-Accuracy Estimations of Frequency, Amplitude, and Phase with a Modified DFT for Asynchronous Sampling. *IEEE Trans. Instrum. Meas.* **2013**, *62*, 1428–1435. [CrossRef]
39. McGrath, B.P.; Holmes, D.G.; Galloway, J.J.H. Power Converter Line Synchronization Using a Discrete Fourier Transform (DFT) Based on a Variable Sample Rate. *IEEE Trans. Power Electron.* **2005**, *20*, 877–884. [CrossRef]
40. Orallo, C.M.; Carugati, I.; Maestri, S.; Donato, P.G.; Carrica, D.; Benedetti, M. Harmonics Measurement with a Modulated Sliding Discrete Fourier Transform Algorithm. *IEEE Trans. Instrum. Meas.* **2014**, *63*, 781–793. [CrossRef]
41. Frigo, G.; Derviskadic, A.; Paolone, M. Reduced Leakage Synchrophasor Estimation: Hilbert Transform Plus Interpolated DFT. *IEEE Trans. Instrum. Meas.* **2019**, *68*, 3468–3483. [CrossRef]
42. Borkowski, J.; Kania, D.; Mroczka, J. Interpolated-DFT-Based Fast and Accurate Frequency Estimation for the Control of Power. *IEEE Trans. Ind. Electron.* **2014**, *61*, 7026–7034. [CrossRef]
43. Kamwa, I.; Samantaray, S.R.; Joos, G. Wide Frequency Range Adaptive Phasor and Frequency PMU Algorithms. *IEEE Trans. Smart Grid* **2014**, *5*, 569–579. [CrossRef]
44. Roscoe, A.J.; Abdulhadi, I.F.; Burt, G. P and M Class Phasor Measurement Unit Algorithms Using Adaptive Cascaded Filters. *IEEE Trans. Power Deliv.* **2013**, *28*, 1447–1459. [CrossRef]
45. Wang, M.; Sun, Y. A Practical Method to Improve Phasor and Power Measurement Accuracy of DFT Algorithm. *IEEE Trans. Power Deliv.* **2006**, *21*, 1054–1062. [CrossRef]
46. Wang, M.; Sun, Y. A Practical, Precise Method for Frequency Tracking and Phasor Estimation. *IEEE Trans. Power Deliv.* **2004**, *19*, 1547–1552. [CrossRef]



© 2020 by the authors. Licensee MDPI, Basel, Switzerland. This article is an open access article distributed under the terms and conditions of the Creative Commons Attribution (CC BY) license (http://creativecommons.org/licenses/by/4.0/).